




Rapid viscoelastic spreading

Ambre Bouillant , Pim J. Dekker , Michiel A. Hack , and Jacco H. Snoeijer
Physics of Fluids Group, Mesa+ Institute, University of Twente, 7500 AE Enschede, The Netherlands



(Received 11 July 2022; accepted 12 December 2022; published 30 December 2022)

We investigate the rapid spreading dynamics of a viscoelastic drop on a solid. Upon contact, surface tension drives a fast motion of the contact line along the substrate. Here we resolve this motion for viscoelastic liquids by experiments on aqueous polymer solutions of varying concentration. It is found that while the contact line motion is only mildly affected by the polymers, the interface profile becomes much sharper owing to singular polymer stress. This behavior is reminiscent of that observed for viscoelastic drop coalescence; in this context we revisit the analogy between spreading and coalescence, which sheds light also on the spreading of Newtonian liquids.

DOI: [10.1103/PhysRevFluids.7.123604](https://doi.org/10.1103/PhysRevFluids.7.123604)

I. INTRODUCTION

When a drop comes into contact with a surface, it starts to spread on the solid. A liquid bridge connecting the drop to the substrate moves radially outwards from the contact point, wetting a circular area of radius $r_0(t)$. The fate of the drop after contact has been the subject of numerous studies, focusing both on static and dynamical aspects. The statics deals with the final shape of the drop and ultimate spreading extent, while the dynamics is dedicated to how a contact line moves and how a drop reaches its final state [1–3]. In partial wetting conditions, the equilibrium contact angle θ sets the final shape of the liquid drop. For the most common case of water drops, the combination of limited spreading and low viscosity of the liquid means that the bridge dynamics is resisted by inertia. A balance between the driving capillary effect with the opposing inertia provides the relevant time scale, namely, the inertio-capillary time $\tau = \sqrt{\rho R^3/\gamma}$, where γ denotes the liquid surface tension and ρ , the liquid density. For a water drop with millimetric size R , $\tau \approx 3$ ms. When observed with the naked eye, the drop thus reaches its final shape quasi-instantaneously. In complete wetting conditions, by contrast, the liquid keeps on spreading slowly making it easily observable. This late stage in the spreading of Newtonian liquids was first studied by Tanner [4], who showed that the radius of the wetted area $r_0(t)$ grows as $t^{1/10}$. This slow regime is dominated by strong viscous dissipation close to the moving contact line [4–6]. This law, however, fails to capture the early stages of the spreading dynamics, where the geometry of the liquid bridge is manifestly different from the slender wedge assumption that underlies Tanner’s law.

The rapid spreading that occurs immediately after the drop is brought into contact with spreading was addressed much more recently, starting with Biance *et al.* [7]. They identified a regime at early time ($t < \tau$), where inertia balances capillarity. The size of the wetted area $r_0(t)$ then grows as

$$\frac{r_0}{R} \sim \left(\frac{\gamma}{\rho R^3} \right)^{1/4} t^{1/2} = \left(\frac{t}{\tau} \right)^{1/2}, \quad (1)$$

which naturally involves the inertio-capillary time τ . This initial work focused on hydrophilic substrates that are completely wetting, and was followed by other studies that varied the substrate properties using both experiments and simulations [8–13]. While some works indicated

that properties of the substrate influence the dynamics [8–10], it was found that—at very early times—the spreading dynamics is universal [11,12] and described by the same scaling (1) as for hydrophilic surfaces. Surprisingly, this universal spreading was found to be irrespective of the substrate wettability and nature (whether it be completely or partially wetting, or even soft), and despite the presence of chemical patterns or any roughness (anisotropic, random, or even controlled) [13].

Curiously enough, the spreading law (1) is identical to the growth of the bridge during the coalescence of two drops in the inviscid regime [14–19]. The analogy between rapid spreading and coalescence has proven very robust, both in the low-viscosity limit [7,11,20] and in the viscous limit [12]. Indeed, in both situations, namely, when a drop is brought into contact with either a solid wall or with another drop, the dynamics evolves through a singular liquid bridge that is vanishingly small at the moment of contact. The success of the spreading-coalescence analogy has been attributed to the fact that the coalescence geometry exhibits a mirror plane that mimics the role of the substrate in spreading. One should bear in mind, however, that it is not obvious that the flow along the plane of symmetry is similar in both cases, as for the spreading over a substrate one expects the no-slip condition to impede the motion of the contact line [9,10,21]. Still, the spreading-coalescence analogy offers a rationalization as to why rapid drop spreading of Newtonian liquids is insensitive to substrate properties.

In the present study, we investigate the rapid spreading of viscoelastic liquids, focusing on polymer suspensions. Viscoelastic liquids are hybrid materials: they can flow like ordinary liquids, yet respond elastically when excited by rapid deformations [22]. This is illustrated by saliva and most biological fluids are viscoelastic in nature because of the long and flexible polymer chains they contain. When a drop of saliva sandwiched between two fingers is drawn away, it can stretch by several times its radius without breaking, an elastic response that leads to a highly elongated threads [23]. However, when loaded over a long timescale, the same drop flows as a liquid and spreads out on the substrate. This viscoelastic behavior originates from the polymer chains that are dissolved in the Newtonian solvent. At rest, the polymer chains form coils. When stretched by the flow, however, the polymers elongate and exert an additional stress onto the solvent. Once the stretching is turned off, polymers relax back to the coil-like structure, which comes with a characteristic relaxation time λ . Polymers were found to slow down the late spreading of a drop, that is in the regime where Tanner’s law is expected [24]. Viscoelastic liquids are ubiquitous in biofluids and in technologies such as coating, printing, aerosol generation and polymer processing, and their flow raises many challenges. Of particular interest is how viscoelastic liquids behave near singularities [25], such as flows around sharp edges [26–28], bubble cusps [29–31] or during the breakup of drops [23,32–37]. Such flows involve regions of extreme polymer stretching, as is also expected to be the case for rapid viscoelastic spreading.

Here we reveal how the addition of polymers influences the early stages of drop spreading on a solid substrate. Given the spreading-coalescence analogy discussed above, the coalescence of viscoelastic drops naturally serves as a benchmark for rapid viscoelastic spreading [38,39]. Surprisingly, the temporal evolution of the bridge during coalescence was found to be only mildly affected by the addition of polymer [39]: the bridge growth is nearly identical to that for Newtonian fluids of low viscosity [14–18,40,41], and was observed to follow Eq. (1) for spherical drops. However, the spatial features of the coalescing bridges are modified: profiles are sharper and the bridge curvature is enhanced. In the present study, we experimentally probe the rapid spreading of polymeric drops. Specifically, we resolve the spatiotemporal dynamics of the bridge growth, and inquire whether the spreading-coalescence analogy is robust in the context of viscoelastic liquids.

II. EXPERIMENTAL PROCEDURE

Spreading experiments are performed on partially wetting glass substrates by studying drops of polymer solutions of varying concentration c and low viscosities. To that end, we use solutions of polyethylene oxide (PEO, $M_w = 4.0 \times 10^6$ g/mol, Sigma-Aldrich) in distilled water. The solution

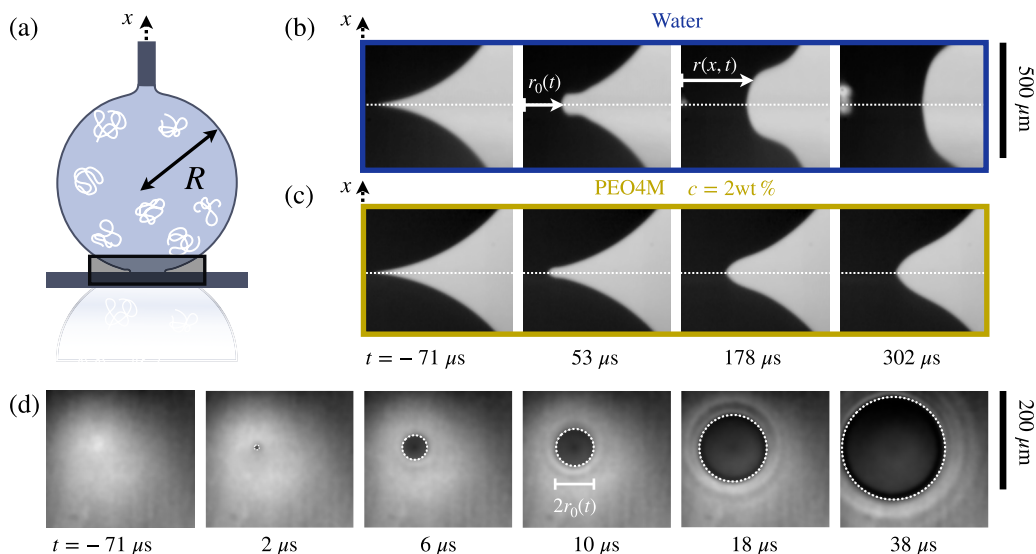


FIG. 1. (a) Side-view schematic of the experimental setup: a drop of PEO is slowly brought into contact with a smooth, transparent and clean glass plate. (b) Upon contact, a water drop rapidly spreads over the solid. The white dashed line indicates the position of the substrate; the lower half of the image is a reflection. The contact line motion is described by the rapid growth of the contact radius r_0 . (c) Spreading of a 2.0 wt % PEO drop. The wetting dynamics is weakly slowed down and the interface profiles are much sharper, as compared to the case of water. The scale bar, common to both series of snapshots, indicates $500 \mu\text{m}$. (d) Series of snapshots taken from below of a water drop spreading on a (transparent) substrate. Prior to contact, the thin air gap separating the drop from the solid produces an interference pattern. After contact, the liquid quickly wets the solid: the dark area expands radially by typically $200 \mu\text{m}$ in $50 \mu\text{s}$, resulting in spreading velocities of about 5 m/s . The scale bar indicates $200 \mu\text{m}$.

concentration is varied from 0.01 to 2.0 wt %, across $c^* \approx 0.1\text{--}1 \text{ wt } \%$, the threshold over which polymer coils start to overlap (see the Supplemental Material [42]). Each solution is mixed with a magnetic stirrer for at least 24 hours and degassed to get rid of air bubbles.

Calibrations of the polymeric solutions used in this study are identical to those in [39], repeated here for completeness in the Supplemental Material [42]. The shear viscosities of the solutions η are measured using a rheometer (MCR 502 with CP50-1, Anton Paar), the surface tension γ and the relaxation times λ are deduced from pendant drop experiments by fitting the drop shape and looking at the thinning of the connecting thread with the dispensing needle [23], respectively. As reported in the SI, the polymer relaxation time λ ranges from 1 to 50 ms in the explored range of concentrations $c = 0.01\text{--}2.0 \text{ wt } \%$, and crosses the inertio-capillary time $\tau = \sqrt{\rho R^3/\gamma} \approx 3 \text{ ms}$. Of particular importance is the values taken at the early stages of spreading of the ratio λ/t , a “local instantaneous Deborah number,” previously defined in [39] which reflects the deformation rate. This number takes values as high as 10^2 up to 10^4 at the smallest timescale resolved in our experiments when the polymer concentration is increased from 0.01 to 2.0 wt %. A strong polymer stretching and elastic effects at the earliest stages of spreading are thus anticipated.

As illustrated in Fig. 1(a), the drop is slowly grown using a dispensing needle connected to a syringe pump (PHD 2000, Harvard Apparatus), pumping at a rate $<0.1 \mu\text{l}/\text{min}$. The needle is placed about 2 mm above the horizontal substrate, in order to produce drops with radius $R \approx 0.9 \text{ mm}$. The deformations induced by the needle are local and far from the contact zone and do not disturb the liquid bridge. The very slow increase in the drop volume enables approach velocities on the order of $1 \mu\text{m}/\text{s}$, that is about three orders of magnitude smaller than typical bridge velocities. Experiments are performed on clean transparent glass slides (supplied by Menzel-Gläser), on which we measure

static advancing contact angles of $52^\circ \pm 4^\circ$. It is well known that the exact nature of the substrate, specifically its wettability, has no influence on the early dynamics of a spreading droplet [11]. Upon contact with the substrate, the liquid spreads. The spreading dynamics is recorded both from the side and from the bottom using synchronized high speed cameras (Nova S12, Photron). The side-view camera is equipped with a zoom lens (Navitar lens), allowing for frame rates ranging from 100 to 200 kfps and a spatial resolution of typically $2 \mu\text{m}/\text{pixel}$. Typical snapshots of the early stage of the spreading of a drop with radius $R = 0.9 \pm 0.1 \text{ mm}$ are shown in Figs. 1(b) and 1(c) for water and for a PEO solution of 2 wt %, respectively. Time increases from left to right with intervals of $125 \mu\text{s}$ between each image. Note that the upper half of the image represents the drop, while the lower half (below the white dotted line) is the reflection in the substrate.

Side views are complemented with synchronized bottom views. The bottom-view camera, mounted on an inverted microscope with a zoom lens (with $10\times$ Olympus lens), shoots at 250 kfps, which enables better spatial and temporal resolutions than for the side view. We display in Fig. 1(d) series of snapshots showing the liquid progression. Prior to contact, the thin air gap separating the drop from the solid produces an interference pattern, where fringes scroll as the drop approaches the substrate. After contact, the liquid quickly wets the solid: the dark area expands radially by approximately $200 \mu\text{m}$ in $50 \mu\text{s}$, resulting in spreading velocities of about 5 m/s .

We focus on the spatiotemporal evolution of the bridge profile, $r(x, t)$, defined in Fig. 1 as the distance parallel to the substrate from the drop vertical axis of symmetry (located in $r = 0$) and the liquid-air interface. We also denote as $r_0(t)$ the radius of the wetted area, which corresponds to $r_0(t) = r(0, t)$. The profiles are extracted using a subpixel interface tracking code. Finding the precise moment of first contact between the drop and the substrate is crucial to determine the growth exponent α . Here $t = 0$ is determined by the bottom view, whose resolution is typically $5 \mu\text{s}$, and further refined by extrapolating a power law $r_0 \propto t^\alpha$, following the protocol as described in [39].

III. RAPID SPREADING DYNAMICS

A. Temporal dynamics

The effect of polymers on the contact radius temporal growth is inconspicuous. Figure 2 presents the temporal evolution of the contact radius $r_0(t)$ for spreading drops of varying polymer concentrations, on both linear [Fig. 2(a)] and logarithmic [Fig. 2(b)] scales. In view of the known behavior for water drops, the horizontal axis is scaled by the inertio-capillary time τ and the vertical axis by the drop radius R . Interestingly, the data exhibit a nearly perfect collapse for all polymer concentrations, especially at early times. Only at later times some differences become apparent. To further quantify this behavior, we fitted the growth of the liquid bridge using a power law of the type $r_0/R = K(t/\tau)^\alpha$. For water, the spreading exponent is known to be $\alpha = 1/2$, while the prefactor reported in literature is $K = 1.2$ [7,11]. The fitted values of α and K in our experiments on polymer solutions are presented in Figs. 2(c) and 2(d), for all tested concentrations. We find that the spreading exponent is consistent with $\alpha = 1/2$, for all polymer concentrations. Likewise, the prefactor K is in close agreement with the value measured for water.

Remarkably, we find that the early stages of spreading of PEO solutions is nearly identical to that of pure water. Even though there is a very rapid motion, which certainly induces large polymer stretching, the temporal dynamics is hardly affected by the presence of polymer. At most, we observe a weak trend for the prefactor K , indicating a minor slowing down. We note that the highest concentration $c = 2 \text{ wt } \%$ departs slightly from the water exponent and prefactor, which can possibly be attributed to the fact that the concentration exceeds the overlapping concentration c^* (estimated around $1 \text{ wt } \%$; see the Supplemental Material [42]); this mixture is clearly not in the dilute regime, which might be the reason why α and K slightly differ from the value observed at lower concentrations.

An important comment to make is that the spreading of PEO solutions is very different from the spreading observed for Newtonian liquids of matching shear viscosity. For example, for

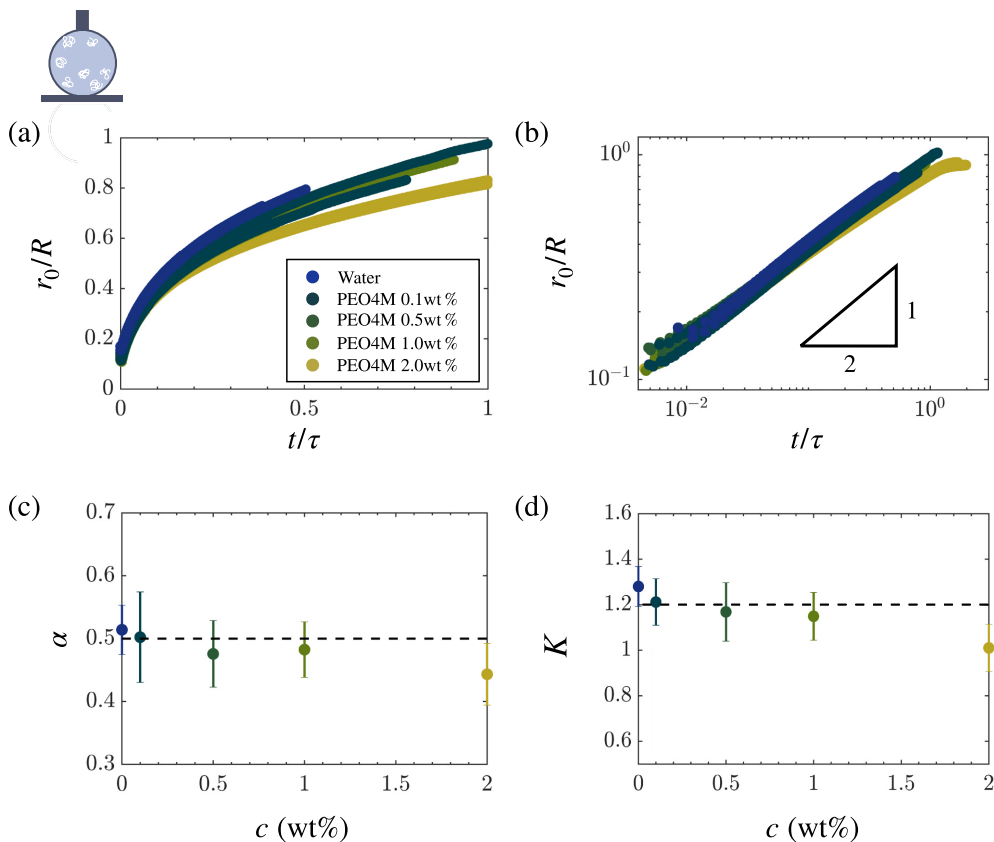


FIG. 2. Temporal spreading dynamics. (a) Contact radius r_0 (scaled by the drop radius R), as a function of time t (scaled by the inertio-capillary time τ) for water and PEO solutions of varying concentrations. (b) Same data on a logarithmic scale. (c) Fitted exponent α extracted from $r_0/R = K(t/\tau)^\alpha$ as a function of c , the PEO concentration; the dashed line indicates the exponent expected for Newtonian liquids, $\alpha = 1/2$. (d) Prefactor K as a function of a function of c ; the dashed line indicates the value expected for Newtonian liquids, $K = 1.2$ [7,11]. The error bars on α and K arise from the averaging different experiments with the same liquid.

$c = 2$ wt%, the solution’s effective viscosity is at max $\eta \approx 10$ Pa s, and the corresponding Newtonian drop would be deeply in the viscous regime. Having said that, we note that the solution is actually shear thinning, so the effective viscosity is thus expected to vary over the spreading process, being maximum at low shear rate. The scaling for rapid drop spreading in the viscous regime is linear with a logarithmic correction, as $r_0 \sim t \ln t$, which would result into apparent spreading exponents close to 0.8 [41]. However, the data in Fig. 2 show no trend towards an increase of the exponent, from the inertial $1/2$ toward the viscous apparent exponent. We thus conclude that in spite of the enhanced shear viscosity of the polymer solutions (at low shear rates), the behavior for α and K remains “inertial” in nature.

B. Spatial structure

Though the *temporal* dynamics of the spreading is hardly affected, the presence of polymer strongly modifies the *spatial* structure of the bridge. This can be seen in Figs. 1(b) and 1(c) and is further evidenced in Fig. 3, where we report the profiles $r(x, t)$ for different times after contact. The profiles appear nearly symmetric in the vertical direction, owing to the reflection in the substrate

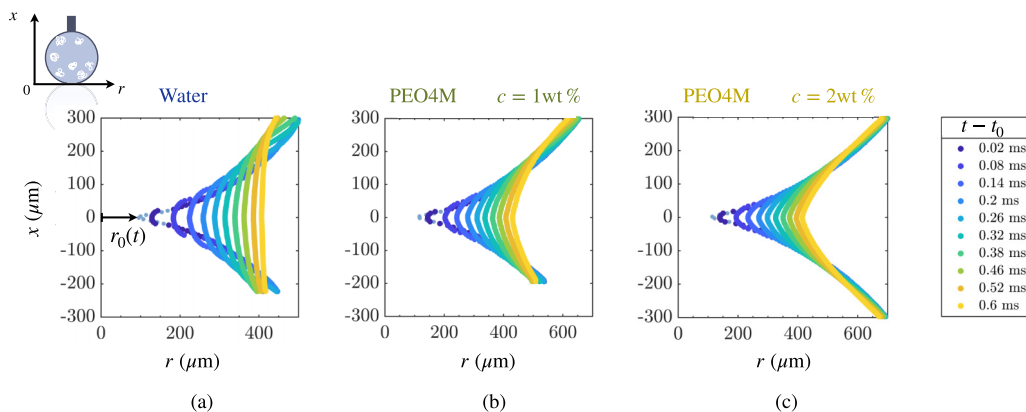


FIG. 3. Evolution of the bridge profiles (including the reflection in the substrate and the profile prior to contact in light blue) for spreading drops of (a) water, (b) PEO with 1 wt %, and (c) PEO with 2 wt %, shown at different times [with $t/\lambda = 0.0007 \rightarrow 0.02$ for panel (b) and $t/\lambda = 0.0003 \rightarrow 0.01$ for panel (c)]. Viscoelastic profiles exhibit a much sharper bridge than water.

that is included in the plot. The viscoelastic bridges are found to be much sharper: while the water profiles are rather shallow [Fig. 3(a)], the interface exhibits a more pronounced curvature ascribed to the addition of polymers [Figs. 3(b) and 3(c)]. Remarkably, this effect is highly localized at the center of the bridge; the effect of polymer fades away at farther distance from the substrate. Though previous works have indicated a possibility that polymer is depleted close to the wall [43,44], the distinct change of bridge morphology implies that polymers remain present inside the bridge.

We now further quantify the sharpness of the bridge. First, we remark that the apparent contact angle of the interface with the substrate is very close to 90° . This can be concluded from plotting $r(x, t)$ as a function of x^2 . This plot gives a purely linear trend without any offset or asymmetry (data available in the Supplemental Material [42]), which confirms that, on the scale of our experimental resolution, the apparent angle cannot be distinguished from 90° . Subsequently, we can quantify the sharpness of the bridge by inspecting the bridge curvature κ close to the substrate. The curvature is defined as $\kappa = r_{xx}(t)$, which can be extracted at each instant from the slope of the curve of $r(x, t)$ vs x^2 , in the vicinity of $x = 0$ (see the Supplemental Material [42]). The curvature is of particular interest, since it gives direct information of the stress inside the liquid, according to Laplace's law of capillarity [45]. Hence, the enhanced curvature is a direct measure for the increase in stress due to polymer stretching.

The resulting $\kappa(t)$ is plotted in Fig. 4, for different concentrations. In Fig. 4(a) the curvature κ is made dimensionless with the drop radius R (normalization with the dominant curvature, R/r_0^2 , is perhaps more natural, but it markedly increases the noise in the data in the limit where $r_0 \rightarrow 0$), while time is scaled with the inertio-capillary time τ . For all concentrations, the bridge curvature is found to decay algebraically, with the smallest curvatures observed for water. The exponent does not appear to take on a distinct universal value, but changes with the nature of the liquid. We see a transition of the exponent from around -1 for water to lower apparent exponents, towards approximately $-1/2$ for the higher PEO concentrations. Note that though rapid spreading of water drops is extensively studied, the bridge curvature is usually not considered; hence we are not aware that the behavior $\kappa \sim 1/t$ for water has been previously reported. In an attempt to account for the viscoelastic nature of the solutions, we also report the data by normalizing time after contact with the polymer relaxation time λ , shown in Fig. 4(b). This scaling gives a much better grouping of the data, which suggests that the dynamics of the curvature is indeed governed by polymer stretching, and its subsequent relaxation. The collapse, however, is not perfect and we could not identify a clear scaling law. When fitting the curvature $\kappa(t)$ with a power law, the exponent is not universal but we find values in a range from -1 to $-1/2$, which remains to be understood.

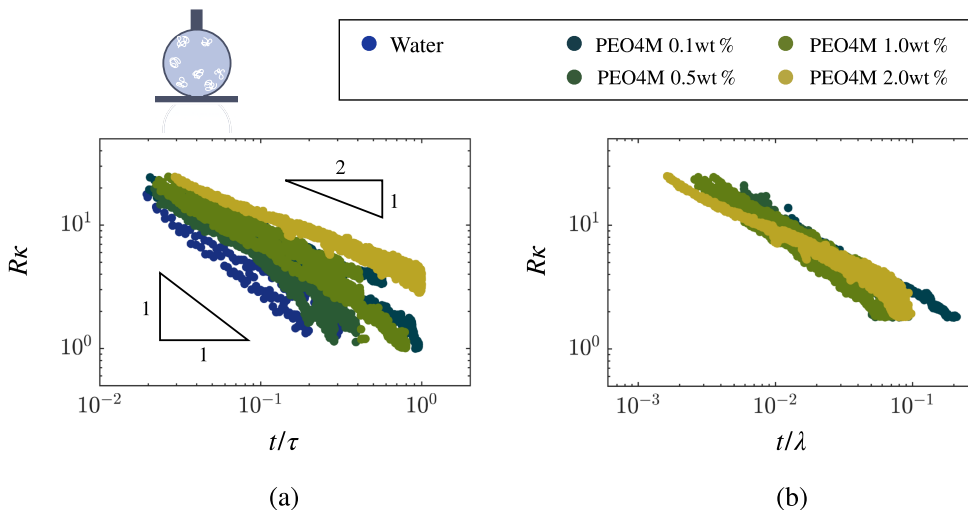


FIG. 4. Bridge curvature κ (normalized by the curvature $1/R$) plotted as a function of time t . (a) Time is normalized by the inertio-capillary time τ . The suggested exponents are indicated as guide for eyes. (b) Same data (excluding water for which the relaxation time λ is not defined), but time is normalized by the polymer relaxation time λ .

IV. THE SPREADING-COALESCENCE ANALOGY REVISITED

We have thus found that the effect of viscoelasticity on rapid drop spreading is rather intricate. On the one hand, polymers hardly affect the motion of the contact line. Specifically, the spreading exponent remains identical to that for the initial spreading of water drops. On the other hand, the shape of the liquid-vapour interface in the bridge is strongly affected, as it exhibits much larger curvatures. This dual spatiotemporal influence of polymers is very strongly reminiscent to that observed recently in viscoelastic coalescence [39]. In what follows we will explore the analogy between rapid spreading and coalescence in the context of viscoelastic drops.

A. Spatiotemporal dynamics of the liquid bridge

We first focus on the time evolution of the bridge radius $r_0(t)$, reported in Fig. 5, for spreading and coalescence. The data for coalescence are taken from the same experiments as those presented in [39]. The results are again presented in dimensionless form, as r_0/R versus t/τ , for drops of water [Fig. 5(a)], PEO with 1 wt % [Fig. 5(b)], and PEO with 2 wt % [Fig. 5(c)]. Clearly, in all cases, the data for coalescence (triangles) fall perfectly on top of the data for spreading (circles). Hence, coalescence and spreading exhibit indistinguishable temporal dynamics, both in the Newtonian and viscoelastic cases. This implies that the presence of the substrate, in particular of the moving contact line, does not seem to have any influence on the wetting dynamics $r_0(t)$ during spreading; irrespectively of the presence of polymers inside the liquid.

On the face of it, the spatial structure of the liquid bridge observed during spreading is also analogous to that observed during coalescence of two drops. As shown in Fig. 6, the bridge profiles during coalescence are sharper when increasing the PEO concentration, in a way that is similar to drop spreading (for comparison see Fig. 3). The two processes thus have in common that the stress inside the bridge is strongly enhanced due to the stretching of the polymer chains.

However, the central bridge curvature $\kappa(t)$ turns out to be essentially different. To make this apparent, we plot the temporal evolution of the curvature during coalescence in Fig. 7, using the same rescalings as in Fig. 4. Let us first focus on the case of pure water. For coalescence, we find

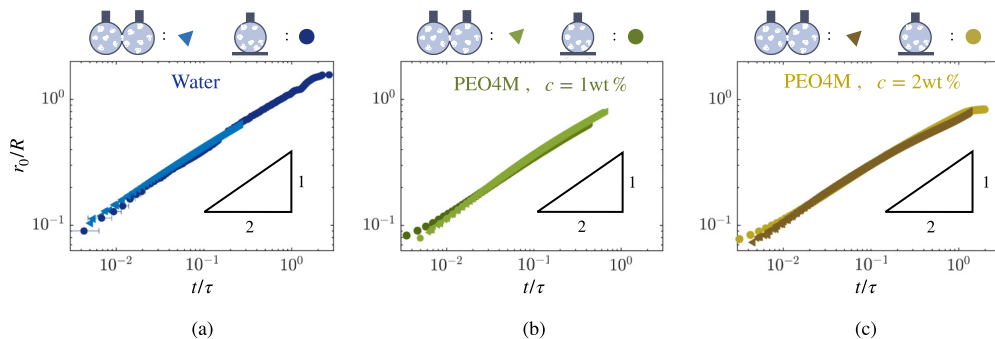


FIG. 5. Direct evidence for the spreading-coalescence analogy for the temporal evolution of the bridge. The three panels directly compare the dynamics of the bridge radius $r_0(t)$ for coalescence (triangles, taken from [39]) and spreading (circles). The data for spreading and coalescence are indistinguishable for (a) water, (b) PEO with 1 wt %, and (c) PEO with 2 wt %.

a scaling behavior that is close to $\kappa \sim 1/t^{3/2}$ [Fig. 7(a)]. However, for spreading of water drops we found $\kappa \sim 1/t$ [Fig. 4(a)]. The curvature data of coalescence clearly does not overlap with that of spreading, which points to a breakdown of the spreading-coalescence analogy. A similar breakdown of the analogy is observed for polymer solutions. For this, one can directly compare Fig. 7(b) and Fig. 4(b), where time is normalized by the polymer relaxation time. For the case of coalescence, it appears that at early times there is a universal scaling $\kappa \sim 1/t$, which again differs substantially from $\kappa(t)$ observed during spreading. Hence, while there is a perfect spreading-coalescence analogy for $r_0(t)$, this analogy does not hold for the local curvatures. This implies that the local stresses at the interface are different for spreading as compared to coalescence.

B. Is the bridge profile self-similar?

To close the discussion on the spreading-coalescence analogy, we finally question whether the dynamics of the liquid bridge exhibits self-similarity. For coalescence of Newtonian drops, it is known that the bridge profiles can be collapsed upon appropriate rescaling of spatial coordinates

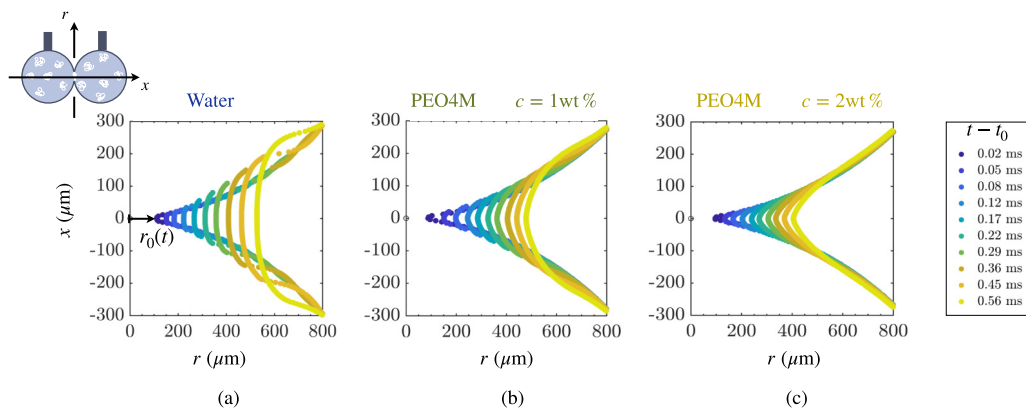


FIG. 6. Evolution of the bridge for coalescing drops of water, PEO with 1 wt %, and PEO with 2 wt %. Bridge profiles (rotated by 90°) are shown at different times matching those in Fig. 3, with $t/\lambda = 0.0007 \rightarrow 0.02$ for 1 wt % PEO and $t/\lambda = 0.0003 \rightarrow 0.01$ for 2 wt % PEO. Viscoelastic solutions exhibit a much sharper bridge than water.

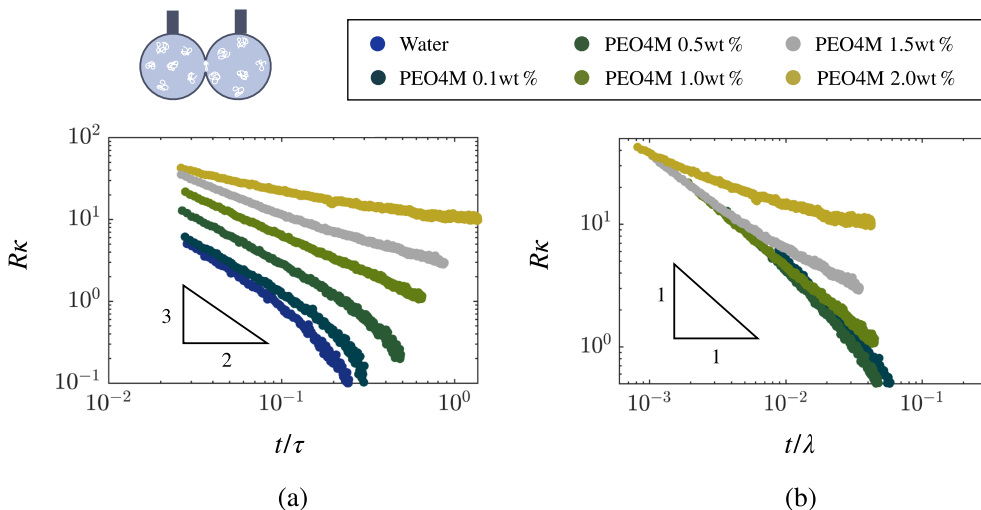


FIG. 7. Coalescence bridge curvature κ (normalized by the drop radius R) plotted as a function of time t . (a) Time is normalized by the inertio-capillary time τ . (b) Same data, but time is normalized by the polymer relaxation time λ .

with time. Specifically, the scaling of the radial coordinate $r/r_0(t)$ and the axial coordinate $xR/r_0^2(t)$ gives a collapse of profiles of coalescing water drops [41]. In Fig. 8 we therefore represent the spatiotemporal evolution of the bridge in viscoelastic spreading and coalescence according to this Newtonian scaling.

We first focus on the case of pure water (left column of Fig. 8). Profiles for *water coalescence* nicely collapse (top-left panel), demonstrating that the dynamics is indeed self-similar. Specifically, the bridge profile follows a dynamics given by $r(x, t) = r_0 \mathcal{H}(xR/r_0^2)$, where \mathcal{H} is a universal function. This also explains the observed scaling of the curvature found for water coalescence. Namely, differentiating $r(x, t)$ twice with respect to x , one finds $\kappa \sim R^2/r_0^3$, which, together with $r_0 \sim t^{1/2}$, leads to the scaling $\kappa \sim 1/t^{3/2}$. Such a self-similarity is however not observed for *water spreading* (bottom-left panel). We recall that in this case, we measured $\kappa \sim 1/t$, which explains why the attempted rescaling in Fig. 8 naturally fails. This lack of self-similarity confirms that the spreading-coalescence analogy breaks down, even for water drops, when considering the spatial structure of the bridge. The analogy only works with respect to the temporal characteristics of the liquid bridge $r_0(t)$, but spreading and coalescence are spatially not equivalent. This points to a difference in the stress inside the liquid bridge. A possible explanation for this differences lies in the flow structure inside the bridge: for coalescence this flow is predominantly extensional in nature, while for spreading the solid will introduce a boundary layer of thickness δ . Such a boundary layer introduces a length scale that could be the cause of the breakdown of self-similarity observed for water coalescence. The presence of a boundary layer actually offers an explanation for the curvature scaling $\kappa \sim 1/t$, as observed during spreading. Namely, we expect the usual scaling for the boundary layer thickness $\delta \sim \sqrt{\nu t}$, where ν is the kinematic viscosity. This implies a shear rate

$$\dot{\gamma} \sim \frac{\dot{r}_0}{\delta} \sim \frac{R}{2t\sqrt{\nu\tau}}, \quad (2)$$

which diverges as $1/t$. Balancing the shear stress $\sigma \sim \eta\dot{\gamma}$ with the Laplace pressure $\gamma\kappa$ then leads to the scaling $\kappa \sim 1/t$. This is in good agreement with the data reported for $\kappa(t)$ in the case of water spreading (see Fig. 4).

We now turn to the case of *viscoelastic coalescence and spreading*. The bridge profile found for viscoelastic drops and shown in the central and right panels in Fig. 8 for both coalescence (upper

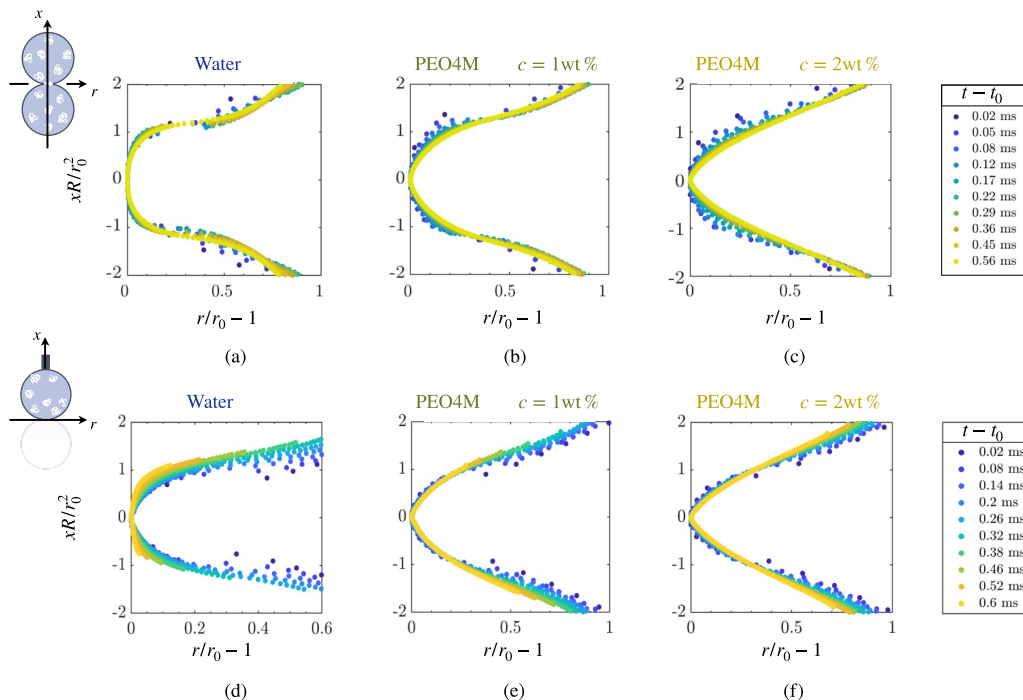


FIG. 8. (a–c) Bridge profiles of coalescing drops of water, PEO with 1 wt % and with 2 wt %, shown at different times, coinciding with Fig. 6. Profiles are rescaled accordingly to the Newtonian self-similar scaling, that is, by normalizing the horizontal and vertical bridge extent r by $r/r_0 - 1$ and x by xR/r_0^2 . (d–f) Bridge profiles of spreading drops of water, PEO with 1 wt % and with 2 wt %, shown at different times, coinciding with Fig. 3, obtained by the same rescaling as in the top row.

plots) and spreading (lower plots), are not self-similar anymore. Indeed, although the water rescaling permits a relative grouping of the profiles, the collapse is less convincing than for water coalescence (top left). In particular, the central region of the bridge does not collapse, which is in line with the differences in scaling of the bridge curvature $\kappa(t)$. A comparable breakdown with respect to the Newtonian self-similarity was found in [39] for the coalescence of *sessile viscoelastic drops*, which are resting on a solid surface before merging. For these sessile drops, the polymer stress was proposed to scale as $\sigma \sim \bar{\eta}_\infty \dot{r}_0/r_0 \sim \bar{\eta}_\infty/t$, where $\bar{\eta}_\infty$ represents the extensional viscosity at high rates. In this specific case, it was found that the presence of polymers by itself introduces a new length scale ℓ that could be found by matching the polymer stress relaxation with the polymer stretch found from a geometrical argument [39]. The self-similar solutions for the sessile geometry were then successfully deduced by balancing the polymer stress, $\bar{\eta}_\infty/t$, with Laplace pressure in the bridge region $\gamma\kappa$. Hence, in the coalescence of sessile viscoelastic drops, the polymer stress in the bridge center gives rise to a different type of self-similarity and dictates how the curvature relaxes with time ($\kappa \sim 1/t$). Figure 7(b) reveals that the scaling $\kappa \sim 1/t$ is preserved in the *coalescence of spherical viscoelastic drops*, suggesting that the same estimate of polymer stress is still applicable here. However, we have not been able any underlying self-similar structure of the bridge profiles; the arguments used for sessile drops (which exhibit a “wedgelike” geometry) do not directly carry over to the more intricate spherical geometry of pendant drops.

Finally, we return to *viscoelastic spreading*, for which Fig. 4 showed that the bridge curvature does not follow an exponent -1 , but exhibits a weaker decay. Given the presence of a shear flow inside the boundary layer, we have therefore explored the possibility that the normal stress difference affects the bridge curvature. PEO solutions are expected to produce a normal stress difference,

denoted as N_1 , that increases quadratically with $\dot{\gamma}$ [37,46,47],

$$N_1 = 2\eta\lambda\dot{\gamma}^2, \quad (3)$$

where we recall that η is the shear viscosity (at low $\dot{\gamma}$) and λ the relaxation time. Combining Eqs. (2) and (3), we get

$$N_1 \sim \frac{\eta\lambda R^2}{2\nu\tau t^2}. \quad (4)$$

The balance between Laplace pressure with this normal stress would thus predict a bridge curvature decay as $\kappa \sim 1/t^2$; this is clearly not consistent with the trend reported in Fig. 4. Hence, the observed curvature during spreading of polymers (and the possibility of an underlying self-similarity) remains an open question for future work.

V. CONCLUSION

We have investigated the rapid spreading dynamics of a viscoelastic drop on a solid substrate, focusing on the spatiotemporal dynamics of the liquid bridge that forms immediately after contact. It was found that the time evolution of the contact radius was almost completely insensitive to the presence of polymer, and closely follows the purely inertial spreading law (1). This, however, does not mean that the polymers do not affect the spreading: the interface profile of the liquid bridge is much sharper than the Newtonian case, owing to singular polymer stress. These observations are of interest for applications such as printing and spray deposition, where polymeric additives can be used to control the impact process.

Our experimental findings for rapid viscoelastic spreading are strongly reminiscent to those observed for viscoelastic drop coalescence. Indeed, just like for Newtonian drops, it is found that the bridge radius $r_0(t)$ is identical when comparing rapid spreading to coalescence. Importantly, however, we have found a key breakdown of the spreading-coalescence analogy. This is most directly appreciated from the bridge profiles in Fig. 8, by comparing the top row (coalescence) to the bottom row (spreading). From these rescaled profiles it can be seen the the bridges for spreading are systematically sharper than for coalescence, pointing to a larger stress inside the bridge. In the case of pure water, we anticipate that this can be attributed to a viscous boundary layer associated to the substrate's no-slip boundary condition. In the case of polymer solutions, this effect could also be due to a viscous boundary layer or due to the enhanced stretching of the polymers by shear. While we have provided an interpretation for the observed curvatures during coalescence, the experimental findings for $\kappa(t)$ during viscoelastic spreading offer an interesting question for future studies. It also remains to be explained why, in all these cases, the temporal growth of the bridge is remarkably insensitive to the singular stress inside the central region of the bridge.

ACKNOWLEDGMENTS

The authors thank Charu Datt and Walter Tewes for fruitful discussions. We acknowledge support from NWO Vici (No. 680-47-63), and from an Industrial Partnership Programme of NWO, cofinanced by Canon Production Printing B. V., University of Twente, and Eindhoven University of Technology.

-
- [1] P.-G. De Gennes, Wetting: Statics and dynamics, *Rev. Mod. Phys.* **57**, 827 (1985).
 - [2] D. Bonn, J. Eggers, J. Indekeu, J. Meunier, and E. Rolley, Wetting and spreading, *Rev. Mod. Phys.* **81**, 739 (2009).
 - [3] J. H. Snoeijer and B. Andreotti, Moving contact lines: Scales, regimes, and dynamical transitions, *Annu. Rev. Fluid Mech.* **45**, 269 (2013).

- [4] L. H. Tanner, The spreading of silicone oil drops on horizontal surfaces, *J. Phys. D* **12**, 1473 (1979).
- [5] O. V. Voinov, Hydrodynamics of wetting, *Fluid Dyn.* **11**, 714 (1976).
- [6] R. G. Cox, The dynamics of the spreading of liquids on a solid surface. Part 1. Viscous flow, *J. Fluid Mech.* **168**, 169 (1986).
- [7] A.-L. Biance, C. Clanet, and D. Quéré, First steps in the spreading of a liquid droplet, *Phys. Rev. E* **69**, 016301 (2004).
- [8] J. C. Bird, S. Mandre, and H. A. Stone, Short-Time Dynamics of Partial Wetting, *Phys. Rev. Lett.* **100**, 234501 (2008).
- [9] A. Carlson, G. Bellani, and G. Amberg, Universality in dynamic wetting dominated by contact-line friction, *Phys. Rev. E* **85**, 045302(R) (2012).
- [10] A. Carlson, G. Bellani, and G. Amberg, Contact line dissipation in short-time dynamic wetting, *Europhys. Lett.* **97**, 44004 (2012).
- [11] K. G. Winkels, J. H. Weijts, A. Eddi, and J. H. Snoeijer, Initial spreading of low-viscosity drops on partially wetting surfaces, *Phys. Rev. E* **85**, 055301 (2012).
- [12] A. Eddi, K. G. Winkels, and J. H. Snoeijer, Short time dynamics of viscous drop spreading, *Phys. Fluids* **25**, 013102 (2013).
- [13] B. B. J. Stapelbroek, H. P. Jansen, E. S. Kooij, J. H. Snoeijer, and A. Eddi, Universal spreading of water drops on complex surfaces, *Soft Matter* **10**, 2641 (2014).
- [14] J. Eggers, J. R. Lister, and H. A. Stone, Coalescence of liquid drops, *J. Fluid Mech.* **401**, 293 (1999).
- [15] L. Duchemin, J. Eggers, and C. Josserand, Inviscid coalescence of drops, *J. Fluid Mech.* **487**, 167 (2003).
- [16] S. T. Thoroddsen, K. Takehara, and T. G. Etoh, The coalescence speed of a pendent and a sessile drop, *J. Fluid Mech.* **527**, 85 (2005).
- [17] D. G. A. L. Aarts, H. N. W. Lekkerkerker, H. Guo, G. H. Wegdam, and D. Bonn, Hydrodynamics of Droplet Coalescence, *Phys. Rev. Lett.* **95**, 164503 (2005).
- [18] J. D. Paulsen, J. C. Burton, and S. R. Nagel, Viscous to Inertial Crossover in Liquid Drop Coalescence, *Phys. Rev. Lett.* **106**, 114501 (2011).
- [19] J. E. Sprittles and Y. D. Shikhmurzaev, A parametric study of the coalescence of liquid drops in a viscous gas, *J. Fluid Mech.* **753**, 279 (2014).
- [20] J. C. Courbin, L. Bird, M. Reyssat, and H. A. Stone, Dynamics of wetting: From inertial spreading to viscous imbibition, *J. Phys.: Condens. Matter* **21**, 464127 (2009).
- [21] P. Johansson and B. Hess, Molecular origin of contact line friction in dynamic wetting, *Phys. Rev. Fluids* **3**, 074201 (2018).
- [22] R. I. Tanner, *Engineering Rheology*, Vol. 52 (Oxford University Press, 2000).
- [23] S. L. Anna and G. H. McKinley, Elasto-capillary thinning and breakup of model elastic liquids, *J. Rheol.* **45**, 115 (2001).
- [24] S. Rafai and D. Bonn, Spreading of non-Newtonian fluids and surfactant solutions on solid surfaces, *Physica A* **358**, 58 (2005).
- [25] M. Renardy, *Mathematical Analysis of Viscoelastic Flows* (SIAM, 2000).
- [26] E. J. Hinch, The flow of an Oldroyd fluid around a sharp corner, *J. Non-Newton. Fluid Mech.* **50**, 161 (1993).
- [27] M. Renardy, The stresses of an upper convected maxwell fluid in a Newtonian velocity field near a re-entrant corner, *J. Non-Newton. Fluid Mech.* **50**, 127 (1993).
- [28] J. D. Evans and D. N. Sibley, Re-entrant corner flows of PTT fluids in the Cartesian stress basis, *J. Non-Newtonian Fluid Mech.* **153**, 12 (2008).
- [29] G. Astarita and G. Apuzzo, Motion of gas bubbles in non-Newtonian liquids, *AIChE J.* **11**, 815 (1965).
- [30] Y. J. Liu, T. Y. Liao, and D. D. Joseph, A two-dimensional cusp at the trailing edge of an air bubble rising in a viscoelastic liquid, *J. Fluid Mech.* **304**, 321 (1995).
- [31] R. Zenit and J. J. Feng, Hydrodynamic interactions among bubbles, drops, and particles in non-Newtonian liquids, *Annu. Rev. Fluid Mech.* **50**, 505 (2018).
- [32] A. V. Bazilevsky, V. M. Entov, and A. N. Rozhkov, Liquid filament microrheometer and some of its applications, in *Third European Rheology Conference and Golden Jubilee Meeting of the British Society of Rheology*, edited by D. R. Oliver (Elsevier Applied Science, 1990), pp. 41–43.

- [33] V. M. Entov and E. J. Hinch, Effect of a spectrum of relaxation times on the capillary thinning of a filament of elastic liquid, *J. Non-Newtonian Fluid Mech.* **72**, 31 (1997).
- [34] Y. Amarouchene, D. Bonn, J. Meunier, and H. Kellay, Inhibition of the Finite-Time Singularity during Droplet Fission of a Polymeric Fluid, *Phys. Rev. Lett.* **86**, 3558 (2001).
- [35] C. Clasen, J. Eggers, M. A. Fontelos, J. Li, and G. H. McKinley, The beads-on-string structure of viscoelastic threads, *J. Fluid Mech.* **556**, 283 (2006).
- [36] J. Eggers, M. A. Herrada, and J. H. Snoeijer, Self-similar breakup of polymeric threads as described by the Oldroyd-B model, *J. Fluid Mech.* **887**, A19 (2020).
- [37] A. Deblais, M. A. Herrada, J. Eggers, and D. Bonn, Self-similarity in the breakup of very dilute viscoelastic solutions, *J. Fluid Mech.* **904**, R2 (2020).
- [38] S. C. Varma, A. Saha, S. Mukherjee, A. Bandopadhyay, A. Kumar, and S. Chakraborty, Universality in coalescence of polymeric fluids, *Soft Matter* **16**, 10921 (2020).
- [39] P. J. Dekker, M. A. Hack, W. Tewes, C. Datt, A. Bouillant, and J. H. Snoeijer, When Elasticity Affects Drop Coalescence, *Phys. Rev. Lett.* **128**, 028004 (2022).
- [40] W. D. Ristenpart, P. M. McCalla, R. V. Roy, and H. A. Stone, Coalescence of Spreading Droplets on a Wettable Substrate, *Phys. Rev. Lett.* **97**, 064501 (2006).
- [41] A. Eddi, K. G. Winkels, and J. H. Snoeijer, Influence of Droplet Geometry on the Coalescence of Low Viscosity Drops, *Phys. Rev. Lett.* **111**, 144502 (2013).
- [42] See Supplemental Material at <http://link.aps.org/supplemental/10.1103/PhysRevFluids.7.123604> for rheological characterization of the solutions and details on the curvature measurements.
- [43] M. J. MacDonald and S. J. Muller, Experimental study of shear-induced migration of polymers in dilute solutions, *J. Rheol.* **40**, 259 (1996).
- [44] H. Ma and M. D. Graham, Theory of shear-induced migration in dilute polymer solutions near solid boundaries, *Phys. Fluids* **17**, 083103 (2005).
- [45] P.-G. de Gennes, F. Brochard-Wyart, and D. Quéré, *Capillarity and Wetting Phenomena: Drops, Bubbles, Pearls, Waves* (Springer, New York, 2004), Vol. 315.
- [46] R. B. Bird, C. F. Curtiss, R. C. Armstrong, and O. Hassager, *Dynamics of Polymeric Liquids* (John Wiley & Sons, 1987).
- [47] D. V. Boger and K. Walters, *Rheological Phenomena in Focus* (Elsevier, 2012).